

# Dominant transport pathways in an atmospheric blocking event

Enrico Ser-Giacomi,<sup>1</sup> Ruggero Vasile,<sup>2</sup> Irene Recuerda,<sup>1</sup> Emilio Hernández-García,<sup>1</sup> and Cristóbal López<sup>1</sup>

<sup>1</sup>*IFISC (CSIC-UIB), Instituto de Física Interdisciplinar y Sistemas Complejos,*

*Campus Universitat de les Illes Balears, E-07122 Palma de Mallorca, Spain*

<sup>2</sup>*Ambrosys GmbH, Albert-Einstein-Str. 1-5, 14473 Potsdam, Germany*

(Dated: 11 October 2024)

A Lagrangian flow network is constructed for the atmospheric blocking of eastern Europe and western Russia in summer 2010. We compute the most probable paths followed by fluid particles which reveal the *Omega*-block skeleton of the event. A hierarchy of sets of highly probable paths is introduced to describe transport pathways when the most probable path alone is not representative enough. These sets of paths have the shape of narrow coherent tubes flowing close to the most probable one. Thus, even when the most probable path is not very significant in terms of its probability, it still identifies the geometry of the transport pathways.

PACS numbers: 92.60.-e, 47.27.ed, 89.75.Hc

**Eastern Europe and Western Russia experienced a strong heat wave with devastating consequences in the summer of 2010. This was due to an atmospheric blocking episode that lasted during several weeks. Despite these type of events have been well-investigated over the years, a complete understanding and prediction is still missing. In this work we present a characterization of this flow pattern based on the study of fluid transport as a Lagrangian flow network, so that the methodology of complex networks can be applied. In particular, the most probable paths linking nodes of this atmospheric network reveal the dominant pathways traced by atmospheric fluid particles.**

## I. INTRODUCTION

Lagrangian analysis of transport in fluids, in particular in geophysical contexts, has experienced intense developments in the last decades. These can be roughly classified in three classes: Some of the approaches search for geometric objects –lines, surfaces, usually related to invariant manifolds – which bound fluid regions with different properties<sup>1–3</sup>. In the second type of approaches one computes different types of Lyapunov exponents and other stretching-like fields in the fluid domain<sup>4–7</sup>. Finally, set-oriented methods<sup>8–12</sup> address directly the motions of finite-size regions.

Most of these techniques focus in identifying proper *Lagrangian Coherent Structures*<sup>13–15</sup>, understood as *barriers to transport* or *coherent regions* with small fluid exchange with the surrounding medium. Much less is known about the actual *routes of transport*, the dominant *pathways* along which fluid particles travel and fluid properties are interchanged.

In principle, the pathways are simply given by trajectories starting from the desired initial conditions. This is true when the advection dynamics is represented by a deterministic dynamical system and the initial condition is precisely fixed. In many applications however,

particularly in geosciences, stochastic components are added to the motions to better represent unresolved spatial scales<sup>16–18</sup>. Also, imprecisely stated initial conditions will develop into a divergent set of possible trajectories, because of the inherently chaotic character of advection by nearly any nontrivial fluid flow. In fact in real experiments such as in the deployment of buoys or balloons the trajectories of closely released objects diverge soon<sup>19–21</sup>. The so-called *spaghetti plots*<sup>18</sup> provide a visual representation of this dispersion. But they become, when many trajectories are represented, cluttered and unclear. Some type of clustering or the selection of relevant trajectories is needed to highlight which are the dominant routes among a large set of possible trajectories.

We have recently developed<sup>22</sup> a formalism that computes the optimal fluid paths starting at given initial conditions and also optimal paths connecting pairs of points. By *optimal* we refer to the paths which are more likely to be followed, in a well-defined sense made explicit below, by the fluid particles initialized in a finite neighborhood of the initial locations. By this reason they are called *most probable paths*. The methodology builds on the set-oriented techniques<sup>8–12</sup> which discretize space to provide a coarse-grained description of transport, and draws analogies with network theory<sup>22–26</sup>, for which tools to compute optimal paths in graphs are well developed. The optimal paths provide the main pathways or skeleton of the transport process in a given geographical area. Because of the implicit stochastic ingredient in the coarse-graining procedure of set-oriented methods, this methodology, at variance with other ones more tied to the theory of smooth dynamical systems, can be applied equally well to cases of deterministic transport and to strongly diffusive situations.

In this paper we compute optimal transport paths for the atmospheric circulation during a blocking event occurring in Summer 2010 (in particular we focus our study for the period 20th July - 30th July) over Eastern Europe and Russia. This atmospheric flow has very different temporal and spatial scales, and is much more diffusive, than the oceanic flow analyzed in Ser-Giacomi et al.<sup>22</sup>. We give a more detailed description of the methodology

sketched in that reference, and generalize it to extend the concept of most probable path to a hierarchy of sets of paths characterized by an increasing probability. The spatial coherence of these sets is also discussed.

The paper is organized as follows: In Sect. II we summarize the definition and construction of the optimal pathways as *most probable paths* in a flow network. In Sect. III we extend this concept to *sets* of highly probable paths and give rules to establish their significance and spatial coherence. Sect. IV describes the atmospheric blocking event, the data and models we use to compute the Lagrangian trajectories and construct the flow network from them. Sect. V contains our results: optimal pathways for different dates and locations, and also a discussion of the statistical representativeness of the optimal paths on the sets of highly probable paths. The final Section summarizes our Conclusions.

## II. OPTIMAL PATHS FROM LAGRANGIAN FLOW NETWORKS

Following the set-oriented methodology<sup>8–12,26</sup> we proceed first by a discretization of the spatial domain of interest, dividing it into  $N$  non-overlapping boxes. In terms of the network-theory approach to transport<sup>22,23,26</sup> each of these boxes will represent a single network *node*. A large number of ideal fluid particles is released in each box. Under advection by a given velocity field, links between nodes are established by studying the Lagrangian trajectories of the particles exchanged among each pair of network nodes. We also need a temporal discretization, i.e. we consider the dynamics restricted to a time interval  $[t_0, t_M]$  and divide it in time steps of length  $\tau$ ,  $t_l = t_0 + l\tau$ ,  $l = 0, 1, \dots, M$ . For each time interval  $[t_{l-1}, t_l]$  we integrate the equations of motion of each ideal fluid particle and keep track of each trajectory. The transport dynamics will then be described by adjacency matrices  $\mathbf{A}^{(l)}$ , ( $l = 1 \dots M$ ), in which a matrix element  $\mathbf{A}_{IJ}^{(l)}$  is given by the number of particles initialized at time  $t_{l-1}$  in node  $I$  that end up at time  $t_l$  in node  $J$ . Since the velocity field will vary in time the adjacency matrices will depend on the time interval considered. The weighted network we build will therefore have an explicit time-dependent character and can be analyzed, for instance, using *time-ordered graphs*<sup>22,27</sup>.

A fundamental assumption we make is that of a Markovian dynamics, i.e. at each time interval the ideal fluid particles are initialized with uniform density in each box, thus without keeping track of the trajectories at the previous time step. The effect of such assumption is to introduce diffusive effects in the dynamics even when the original equations of motion are fully deterministic. In the limit of very small boxes and very short time steps, this computational diffusion is suppressed and we approach the perfect Lagrangian motion under the given velocity field (which itself can contain diffusive or fluctuating terms).

In our network approach spatio-temporal particle trajectories are mapped into discretized paths between the network nodes. We define an  $M$ -step path  $\mu$  between nodes  $I$  and  $J$  as the ordered sequence of  $(M+1)$  nodes,  $\mu = \{I, k_1, \dots, k_{M-1}, J\}$ , crossed to reach node  $J$  at time  $t_M$  starting from node  $I$  at time  $t_0$ . Under the Markovian hypothesis we can associate a probability to each of these paths as

$$(p_{IJ}^M)_\mu = \mathbf{T}_{Ik_1}^{(1)} \left[ \prod_{l=2}^{M-1} \mathbf{T}_{k_{l-1}k_l}^{(l)} \right] \mathbf{T}_{k_{M-1}J}^{(M)}, \quad (1)$$

where

$$\mathbf{T}_{k_{l-1}k_l}^{(l)} = \frac{\mathbf{A}_{k_{l-1}k_l}^{(l)}}{s_{out}^{(l)}(k_{l-1})} \quad (2)$$

is the probability of a fluid particle to reach node  $k_l$  at time  $t_l$  if it was initialized at time  $t_{l-1}$  in node  $k_{l-1}$ , estimated as the ratio of the number of particles doing so to the total number of particles released at the initial node and time. The quantity  $s_{out}^{(l)}(k) = \sum_j \mathbf{A}_{kj}^{(l)}$  is called *out-strength* of node  $k$  during the  $l$ -th time step.

Among all possible  $M$ -step paths between node  $I$  and  $J$  the one associated with the highest probability in Eq. (1) is called the most probable path (MPP) and is denoted by  $\eta_{IJ}^M$ . Its probability is denoted by  $P_{IJ}^M = \max_\mu \{(p_{IJ}^M)_\mu\}$ . To find the MPP and its probability we use an adaptation of the Dijkstra algorithm<sup>28</sup> which takes into account the layered and directed structure of our time-ordered flow graph. In brief, we realize that for on-step paths the maximum probability is  $P_{Ik_1}^1 = \mathbf{T}_{Ik_1}^{(1)}$  and then we apply recursively the formula

$$P_{Ik_{l+1}}^{l+1} = \max_{k_l} \left( P_{Ik_l}^l \mathbf{T}_{k_l k_{l+1}}^{(l+1)} \right) \quad (3)$$

for  $l = 1, 2, M-1$  until reaching the endpoint  $J = k_M$ .

The cost of the computation is reduced by computing the accessibility<sup>29</sup> of each intermediate node at each intermediate time. Once we fix initial and final nodes  $I$  and  $J$  we calculate at each intermediate time which are the nodes that are crossed at least by one path during the dynamics. A given node  $k_l$  at time  $t_l$  is crossed if it is reachable from  $I$  in  $l$  time steps, and at the same time, if from this node it is possible to reach node  $J$  in  $M-l$  time steps. This information is collected in the so-called *accessibility matrices*<sup>29</sup>, which are properly time-ordered products of the network adjacency matrices  $\mathbf{A}$ . Specifically, node  $k$  is contributing at time  $l$  to a path between  $I$  and  $J$  if and only if

$$\left[ \prod_{i=1}^l \mathbf{A}^{(i)} \right]_{Ik} \neq 0 \quad \text{and} \quad \left[ \prod_{i=l+1}^M \mathbf{A}^{(i)} \right]_{kJ} \neq 0. \quad (4)$$

Raising the number  $M$  of steps we observe a fast increase in the number of paths connecting two given nodes. It is thus crucial to understand how much the

MPP is representative of the large set of possible paths joining two nodes. To assess in a quantitative way this issue we introduce the following quantity

$$\lambda_{IJ}^M = \frac{P_{IJ}^M}{\sum_{\mu} (p_{IJ}^M)_{\mu}}, \quad (5)$$

which determines the fraction of probability carried by the MPP with respect to the sum of probabilities of all paths connecting nodes  $I$  and  $J$ . Note that the denominator can be simply computed as the matrix-product entry  $\left(\prod_{l=1}^M \mathbf{T}^{(l)}\right)_{IJ}$ .

### III. SETS OF HIGHLY PROBABLE PATHS

For large values of  $M$ , the MPP progressively loses dominance and, on average, does not carry a significantly high fraction of probability. However the dynamics, characterized by a high number of paths connecting initial and final points, can be still described by a few of them, which together have a non-negligible probability. To see this we can relax the definition of MPP and define a family of subsets of highly probable paths (HPP) holding most of the probability. In our formulation each subset  $\mathcal{K}_{IJ}^M(r, \epsilon)$  is characterized by a *rank*  $0 \leq r \leq M-1$  and a threshold parameter  $0 \leq \epsilon \leq 1$ . Ideally the sets would contain all the paths whose probability is larger than  $\epsilon P_{IJ}^M$ . But since exhaustive searching of all such paths becomes computationally prohibitive except for very small  $M$ , the second parameter  $r$  is introduced to determine the number of constraints imposed in the search for these relevant paths. Given the initial ( $I$ ) and final ( $J$ ) points we fix  $r$  nodes at intermediate times and look for paths between  $I$  and  $J$  made of segments which are MPP's connecting these intermediate nodes, by using the algorithm above. Different locations and times for these  $r$  intermediate nodes are scanned and paths with probability larger than  $\epsilon P_{IJ}^M$  are retained and incorporated into the set  $\mathcal{K}_{IJ}^M(r, \epsilon)$ . For  $\epsilon \rightarrow 1$ , independently on the rank (or for  $r = 0$ ) only the MPP is retained.  $\mathcal{K}_{IJ}^M(r = M-1, \epsilon)$  contains all the paths with probability larger than  $\epsilon P_{IJ}^M$ . However, evaluation of these sets of HPPs can be computationally costly for high values of  $r$ , since the algorithm scales exponentially with  $r$ . Nevertheless interesting results can be obtained considering already low-order HPPs, i.e.  $r = 1$  and  $r = 2$ .

Once one of the subsets is computed we can establish its significance by defining an extension of expression Eq. (5):

$$\lambda_{IJ}^M(r, \epsilon) = \frac{\sum_{\nu} (p_{IJ}^M)_{\nu}}{\sum_{\mu} (p_{IJ}^M)_{\mu}}, \quad (6)$$

where the sum in the numerator is over all the paths in the subset  $\mathcal{K}_{IJ}^M(r, \epsilon)$  and the one in the denominator is over all paths connecting  $I$  to  $J$ .

Another important aspect of the sets of HPPs is to establish how close, spatially, are they with respect to the corresponding MPP. This is obtained with an average distance function. Given two generic paths between initial and final points  $I$  and  $J$ ,  $\mu_1 = \{I, k_1, \dots, J\}$  and  $\mu_2 = \{I, l_1, \dots, J\}$  we define their average distance as

$$\mathbf{d}(\mu_1, \mu_2) = \frac{1}{M-1} \sum_{i=1}^{M-1} d(k_i, l_i), \quad (7)$$

where  $d(k_i, l_i)$  is a metric determining the distance between two given nodes of the network. For a geophysical transport network the geographical distance (on the sphere) between the centers of the nodes is the most natural choice. For a given pair of nodes ( $I, J$ ) the average distance between the subset  $\mathcal{K}_{IJ}^M(r, \epsilon)$  and the MPP connecting them in  $M$  time steps is defined as

$$\mathcal{D}_{IJ}^M = \frac{1}{N_{IJ}^M} \sum_{\mu} \mathbf{d}(\mu, \eta_{IJ}^M), \quad (8)$$

where  $N_{IJ}^M$  is the number of paths  $\mu$  in the subset  $\mathcal{K}_{IJ}^M(r, \epsilon)$ , and the sum is extended over all paths in the subset (remember that  $\eta_{IJ}^M$  denotes the MPP). This quantity provides an estimation of how much paths in the subset deviate spatially from the correspondent MPP. A large deviation means that the probability to reach  $J$  from  $I$  is spatially spread in a large region and indicates furthermore the importance of considering the HPP subset instead of only the MPP. Small values of  $\mathcal{D}_{IJ}^M$  imply HPP sets with the shape of coherent narrow tubes around the MPP, so that the MPP already characterizes the spatial pathways, even if its probability is not large.

### IV. A NETWORK OF ATMOSPHERIC FLOW OVER EASTERN EUROPE IN SUMMER 2010

In this section we describe the physical characteristics of the atmospheric event, the data used and the model we employ to obtain the air particle trajectories.

#### A. Event description

Eastern Europe and Western Russia experienced a strong, unpredicted, heat wave during the summer of 2010. Extreme temperatures resulted in over 50000 deaths and inflicting large economic losses to Russia. The heat wave was due to a strong atmospheric blocking that persisted over the Euro-Russian region from late June to early August<sup>30</sup>. During July the daily temperatures were near or above record levels and the event covered Western Russia, Belarus, Ukraine, and the Baltic nations. Physically, the origins of this heat wave were in a atmospheric block episode that produced anomalously stable anticyclonic conditions, redirecting the trajectories of migrating cyclones. Atmospheric blocks can remain in place

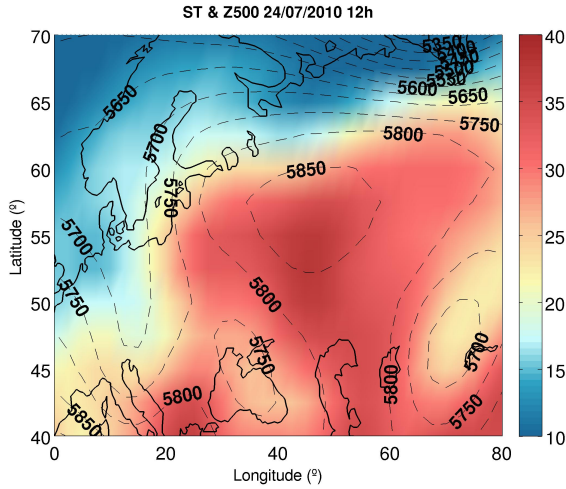


FIG. 1. Geopotential height at 500hPa (contours, in m) and temperature (color code, in degrees C) on July 24th, 12:00 UTC.

for several days (sometimes even weeks) and are of large scale (typically larger than 2000 km). In particular, the Russian block of summer 2010 was morphologically of the type known as *Omega block* that consists in a combination of low-high-low pressure fields with geopotential lines resembling the Greek letter  $\Omega$  (see Fig.1). *Omega blocks* bring warmer and drier conditions to the areas that they impact and colder, wetter conditions in the upstream and downstream<sup>31</sup>. We study the concrete period extended from the July the 20th to July 30th.

## B. Data

Atmospheric data were provided by the National Centers for Environmental Prediction (NCEP) Climate Forecast System Reanalysis (CFSR) through the Global Forecast System (GFS)<sup>32</sup>. This reanalysis was initially completed over the 31 year period from 1979 to 2009 and extended to March 2011. Data can be obtained with a temporal resolution of 1 hour and a spatial horizontal resolution of  $0.5^\circ \times 0.5^\circ$ . The spatial coverage contains a range of longitudes of  $0^\circ E$  to  $359.5^\circ E$  and latitudes of  $90^\circ S$  to  $90^\circ N$ .

The variables needed as input to the Lagrangian dispersion model described in the next section include dew point temperature, geopotential height, land cover, planetary boundary layer height, pressure and pressure reduced to mean sea level, relative humidity, temperature, zonal and meridional component of the wind, vertical velocity and water equivalent to accumulated snow depth. All these fields are provided by CFSR data on 26 pressure levels.

## C. Lagrangian Particle Dispersion Model FLEXPART

As mentioned, the idea is to obtain the effective velocity field felt by any fluid particle. Then the Lagrangian dispersion model (see next subsection) will integrate it to provide as output the three-dimensional positions of the particle at every time step.

The numerical model used to integrate particle velocities and obtain trajectories is the Lagrangian particle dispersion model FLEXPART version 8.2<sup>33,34</sup>. FLEXPART simulates the long-range and mesoscale transport, diffusion, dry and wet deposition, and radioactive decay of tracers released from point, line, area or volume sources. It most commonly uses meteorological input fields from the numerical weather prediction model of the European Centre for Medium-Range Weather Forecasts (ECMWF) as well as the Global Forecast System (GFS) from NCEP (the one used in our study). Trajectories are produced by integrating the equation (the input velocity data are interpolated on the present particle position):

$$\frac{d\mathbf{X}}{dt} = \mathbf{v}(\mathbf{X}(t)), \quad (9)$$

with  $t$  being time,  $\mathbf{X}$  the vector position of the air particle, and  $\mathbf{v} = \bar{\mathbf{v}} + \mathbf{v}^t + \mathbf{v}^m$  is the wind vector. FLEXPART takes the grid scale wind  $\bar{\mathbf{v}}$  from the CFSR, but complements it with stochastic components  $\mathbf{v}^t$  and  $\mathbf{v}^m$  to better simulate the unresolved turbulent processes occurring at small scales. The turbulent wind fluctuations  $\mathbf{v}^t$  are parametrized by assuming a Markov process via a Langevin equation, and the mesoscale wind fluctuations  $\mathbf{v}^m$  are implemented also via an independent Langevin equation by assuming that the variance of the wind at the grid scale provides information on the subgrid variance. Variables entering the parametrizations are obtained from the meteorological CFSR fields. For additional details we refer to Stohl et al.<sup>33,34</sup>.

## D. Network construction

We focus our analysis on the domain in between  $0^\circ E$  -  $80^\circ E$  and  $40^\circ N$  -  $70^\circ N$ . In order to define the nodes of the network we discretize this region in 626 equal-area boxes using a sinusoidal projection. The latitudinal extension of each node-box is  $1.5^\circ$ , the longitudinal one varies depending on the latitude (see Fig. 2). The area of each box is  $27722 \text{ km}^2$ , so that the typical horizontal size is of the order of  $166.5 \text{ km}$ . We take  $\tau = 12$  hours as time discretization. We uniformly fill each node with 800 ideal fluid particles releasing them at  $5000 \text{ m}$  of height, a representative level in the middle troposphere. FLEXPART trajectories are fully three-dimensional, but by initializing at each time-step particles in a single layer we are effectively neglecting the vertical dispersion (which is of the order of  $800 \text{ m}$  in the  $\tau = 12 \text{ h}$  time step) and focussing on the pathways of large scale horizontal transport. Fully

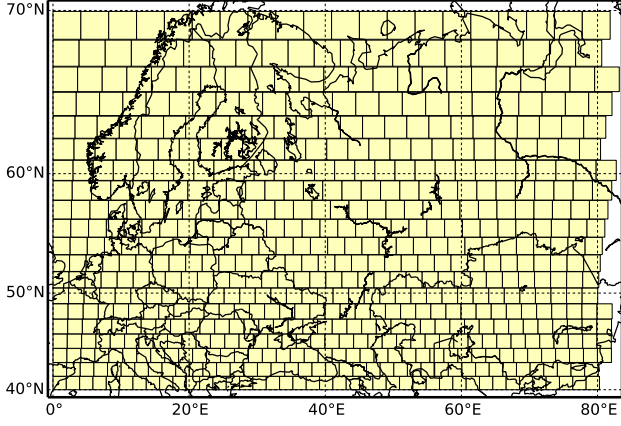


FIG. 2. The geographical domain considered and the discretization grid defining the nodes of our flow network.

three-dimensional flow networks will be the subject of future work.

## V. RESULTS

### A. Optimal paths

Equipped with the tools developed above we can now compute pathways of transport during the atmospheric event described in Sect. IV. Figure 3a shows all the optimal paths leaving a node in the Scandinavian Peninsula at July 25 and arriving to all nodes which are reached in  $M = 9$  steps (i.e. 4.5 days). The graphical representation joins with maximal arcs the center of the grid boxes identified as pertaining to the MPP. The actual particle trajectories between two consecutive boxes are not necessarily such arcs. The paths are colored according to their probability value  $P_{IJ}^M$ . The MPPs with highest probability (reddish colors) follow a dominant anticyclonic (i.e. clockwise) route bordering the high pressure region (see Fig. 1, but note that this is at a particular time, whereas the trajectory plots span a range of dates of more than four days) without penetrating it. There is also a branch of MPPs with much smaller probabilities (yellow and bluish colors) that are entrained southward by a cyclonic circulation.

Despite the persistent character of the Eulerian block configuration, sets of Lagrangian trajectories become highly variable in time. See for example the set of MPPs starting from the same initial location but five days earlier (Fig. 3b). The southward cyclonic branch is now absent, all MPPs following initially the anticyclonic gyre. Remarkably, the set of trajectories bifurcates into two branches when approaching what seems to be a strong hyperbolic structure close to 40°N 60°E. A hint of the presence of second hyperbolic structure is visible at the end of the westward branch, close to 50°N 30°E. Figure

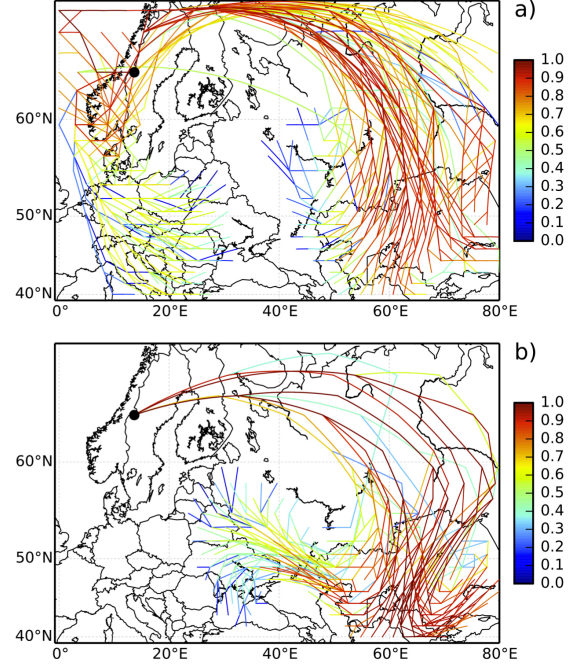


FIG. 3. Paths of  $M = 9$  steps of  $\tau = 12$  hours in our flow network with starting date July 25th 2010 (panel a)) and July 20th 2010 (panel b)), represented as straight segments joining the path nodes. MPPs originating from a single node (black circle) and ending in all accessible nodes. Color gives the  $P_{IJ}^M$  value of the paths in a normalized log-scale between the minimum value (deep blue) and the maximum (dark red). Panel a): probabilities ranging from  $10^{-3}$  to  $10^{-14}$ . Panel b): probabilities ranging from  $10^{-3}$  to  $10^{-15}$ .

4 displays additional MPPs starting also at July 20th, but initialized inside the main anticyclonic region of the blocking, and in two low-pressure regions flanking it. Fig. 4a clearly shows the main anticyclonic circulation, highlighting also the escape routes from the high-pressure zone, associated with the hyperbolic regions described above. The other two panels show the cyclonic circulations at each side of the high, in a characteristic Omega-blocking configuration. It is remarkable the compactness of the trajectories inside the eastern low-pressure area, which form a very localized and coherent set with practically no escape in the 4.5 days time-interval displayed.

We stress that the plots in Figs. 3 and 4 are different from *spaghetti plots* for which many available trajectories are plotted from different or related initial conditions. For our set of particles this will give 800 trajectories emanating from each box. Here we are plotting just one path, the MPP, for each initial and final box pair, which

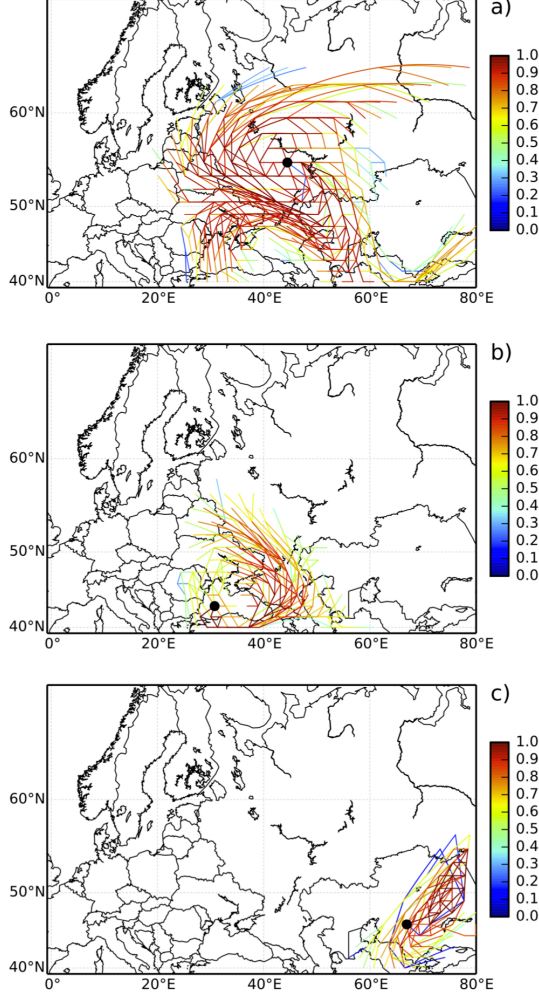


FIG. 4. Optimal paths of 9 steps of  $\tau = 12$  hours with starting date July 20th 2010, entrained in the high- and in the two low-pressure areas of the blocking. Same coloring scheme as in Fig. 3. Panel a): probabilities ranging from  $10^{-3}$  to  $10^{-16}$ . Panel b): probabilities ranging from  $10^{-2}$  to  $10^{-16}$ . Panel c): probabilities ranging from  $10^{-3}$  to  $10^{-13}$ .

strongly limits the number of paths from each box but, as we will see more thoroughly, it is still representative of the trajectories of many released particles.

## B. Relevance of the MPPs

The range of colors in Figs. 3 and 4 indicates that, given an initial box, not all MPPs leading to different locations are equally probable. This is quantified by the probability  $P_{IJ}^M$  which gives a weight to each MPP. Indeed  $P_{IJ}^M$  takes a very large range of values. Figure 5 shows a ranking plot in which the values of all MPPs of a given  $M$  and started at a particular date are plotted in decreasing order. We see a huge spread on the values

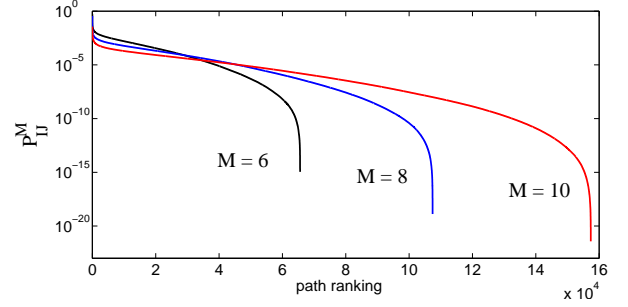


FIG. 5. Ranking plot in which the  $P_{IJ}^M$  values of all MPPs obtained for  $M = 6, 8$ , and  $10$  starting on July 25th in the whole area are plotted in decreasing order. The range of probability values of the MPPs can be read from the vertical axis (from a few percent to  $10^{-15}$  for  $M = 6$  or to less than  $10^{-20}$  for  $M = 10$ ). The total number of optimal paths can also be read-off from the horizontal axis.

of  $P_{IJ}^M$ . Very low probability values arise because of the exponential explosion of the number of paths between two nodes with increasing  $M$ . Given these low values of  $P_{IJ}^M$  except for the smallest values of  $M$ , one should ask how representative are the MPPs for the full set of paths. Figure 6a shows distributions of the parameter  $\lambda_{IJ}^M(r, \epsilon)$  giving the relative importance of the different types of paths. We see that  $\lambda$ -values are small when considering only the MPPs ( $r = 0$ ), but the distributions shift towards higher values for paths sets of increasing  $r$ . Figure 6b gives mean values of the  $\lambda$  distributions. They decrease with  $M$ , reflecting the lack of representativeness of the smallest sets of paths for large  $M$ . However, already for  $r = 1$  the set of HPPs has a mean value higher than 0.5 for a relevant range of time steps.

Thus, for the values of  $M$  and  $\epsilon$  discussed here, the set of HPPs with  $r = 1$  seems to be rich enough to represent the transport pathways. But how different is the geometry of the different paths in this HPP set? And how different is it from the MPPs? We plot in Fig. 7 examples of all HPPs with  $r = 1$  and  $\epsilon = 0$  for particular  $(I, J)$  values and dates. Changing  $M$  changes the shape of the path, but in all the cases the sets remain coherent and narrow tubes of trajectories defining roughly the same pathway as the MPP.

A quantification of the *width* of the tubes can be done with the distance measure  $\mathcal{D}_{IJ}^M$  in Eq. (8). An average of it over pairs of locations is shown in Fig. 8. Although the tube width increases with  $M$ , it remains always below the typical linear box size of approximately 166.5 km (see Sect. IV D) indicating that the tubes remain narrow. Thus we conclude that, despite the decreasing probability of the MPPs for increasing  $M$ , they remain good indicators of the dominant pathways in the transport network.

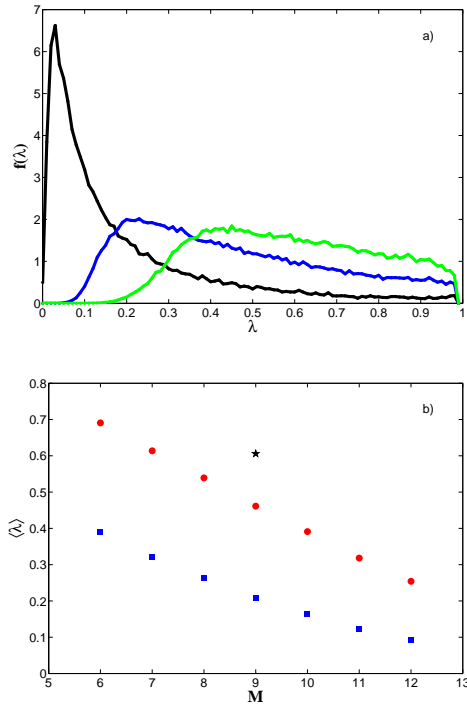


FIG. 6. a) Normalized probability density  $f(\lambda)$  of the merit figure  $\lambda_{IJ}^M(r, \epsilon)$  of paths started on July 20th 2010 for  $M = 9$  and  $\epsilon = 0.1$ , with  $r = 0$  (only the MPPs, black curve),  $r = 1$  (blue) and  $r = 2$  (green). b) Mean value of the  $\lambda_{IJ}^M(r, \epsilon)$  distributions (paths' starting date July 25th) as a function of the number of time steps  $M$  for  $r = 0$  (only MPPs, blue squares),  $r = 1$  (red circles) and  $r = 2$  (single black star).

## VI. CONCLUSIONS

We have introduced MPPs and sets of HPPs as tools to visualize and analyze dominant pathways in geophysical flows. We have computed them for an atmospheric blocking event involving eastern Europe and Western Russia. The computed optimal paths give a Lagrangian view of the Omega-block configuration, with a central anti-cyclonic circulation flanked by two cyclonic ones. Moreover they give additional insight on it, such as the variability of the dominant pathways, and the identification of escaping and trapping regions. The statistical significance of single MPPs decreases with the time interval considered, but we find always that the MPPs remain representative of the spatial geometry of the pathways, in the sense that the sets of HPPs are coherent narrow tubes providing transport paths always close to the optimal path. This spatial coherence of transport between pairs of locations was already noticed in an ocean flow<sup>22</sup> and seems to be a general characteristic of geophysical flow networks.

## ACKNOWLEDGMENTS

We acknowledge financial support from FEDER and MINECO (Spain) through the ESCOLA (CTM2012-39025-C02-01) and INTENSE@COSYP (FIS2012-30634) projects, and from European Commission Marie-Curie ITN program (FP7-320 PEOPLE-2011-ITN) through the LINC project (no. 289447).

- <sup>1</sup>A. M. Mancho, D. Small, and S. Wiggins, "A tutorial on dynamical systems concepts applied to Lagrangian transport in oceanic flows defined as finite time data sets: Theoretical and computational issues," *Physics Reports* **437**, 55–124 (2006).
- <sup>2</sup>G. Haller and F. J. Beron-Vera, "Geodesic theory of transport barriers in two-dimensional flows," *Physica D: Nonlinear Phenomena* **241**, 1680 – 1702 (2012).
- <sup>3</sup>S. Balasuriya, "Explicit invariant manifolds and specialised trajectories in a class of unsteady flows," *Physics of Fluids* **24**, 127101 (2012).
- <sup>4</sup>G. Haller, "Distinguished material surfaces and coherent structure in three-dimensional fluid flows," *Physica D* **149**, 248–277 (2001).
- <sup>5</sup>B. Joseph and B. Legras, "Relation between Kinematic Boundaries, Stirring, and Barriers for the Antarctic Polar Vortex," *J. Atm. Sci.* **59**, 1198–1212 (2002).
- <sup>6</sup>F. d'Ovidio, V. Fernandez, E. Hernandez-García, and C. Lopez, "Mixing structures in the Mediterranean Sea from Finite-Size Lyapunov Exponents," *Geophys. Res. Lett.* **31**, L17203 (2004).
- <sup>7</sup>A. M. Mancho, S. Wiggins, J. Curbelo, and C. Mendoza, "Lagrangian descriptors: A method for revealing phase space structures of general time dependent dynamical systems," *Communications in Nonlinear Science and Numerical Simulation* **18**, 3530–3557 (2013).
- <sup>8</sup>G. Froyland and M. Dellnitz, "Detecting and locating near-optimal almost-invariant sets and cycles," *SIAM Journal on Scientific Computing* **24**, 1839–1863 (2003).
- <sup>9</sup>M. Dellnitz, G. Froyland, C. Horenkamp, K. Padberg-Gehle, and A. Sen Gupta, "Seasonal variability of the subpolar gyres in the Southern Ocean: a numerical investigation based on transfer operators," *Nonlinear Processes in Geophysics* **16**, 655–663 (2009).
- <sup>10</sup>G. Froyland, N. Santitissadeekorn, and A. Monahan, "Transport in time-dependent dynamical systems: Finite-time coherent sets," *Chaos: An Interdisciplinary Journal of Nonlinear Science* **20**, 043116 (2010).
- <sup>11</sup>Z. Levnajić and I. Mezić, "Ergodic theory and visualization. I. Mesochronic plots for visualization of ergodic partition and invariant sets," *Chaos: An Interdisciplinary Journal of Nonlinear Science* **20**, 033114 (2010).
- <sup>12</sup>G. Froyland, C. Horenkamp, V. Rossi, N. Santitissadeekorn, and A. S. Gupta, "Three-dimensional characterization and tracking of an agulhas ring," *Ocean Modelling* **52**, 69–75 (2012).
- <sup>13</sup>G. Haller and G. Yuan, "Lagrangian coherent structures and mixing in two-dimensional turbulence," *Physica D* **147**, 352–370 (2000).
- <sup>14</sup>T. Peacock and J. Dabiri, "Introduction to Focus Issue: Lagrangian coherent structures," *Chaos* **20**, 017501 (2010).
- <sup>15</sup>G. Haller, "Lagrangian coherent structures," *Annual Review of Fluid Mechanics* **47**, 137–162 (2015).
- <sup>16</sup>D. J. Thomson, "Criteria for the selection of stochastic models of particle trajectories in turbulent flows," *Journal of Fluid Mechanics* **180**, 529–556 (1987).
- <sup>17</sup>A. Stohl, "Computation, accuracy and applications of trajectories: a review and bibliography," *Atmospheric Environment* **32**, 947–966 (1998).
- <sup>18</sup>M. Veneziani, A. Griffa, A. M. Reynolds, and A. J. Mariano, "Oceanic turbulence and stochastic models from subsurface lagrangian data for the northwest atlantic ocean," *J. Phys. Oceanogr.* **34**, 1884–1906 (2004).

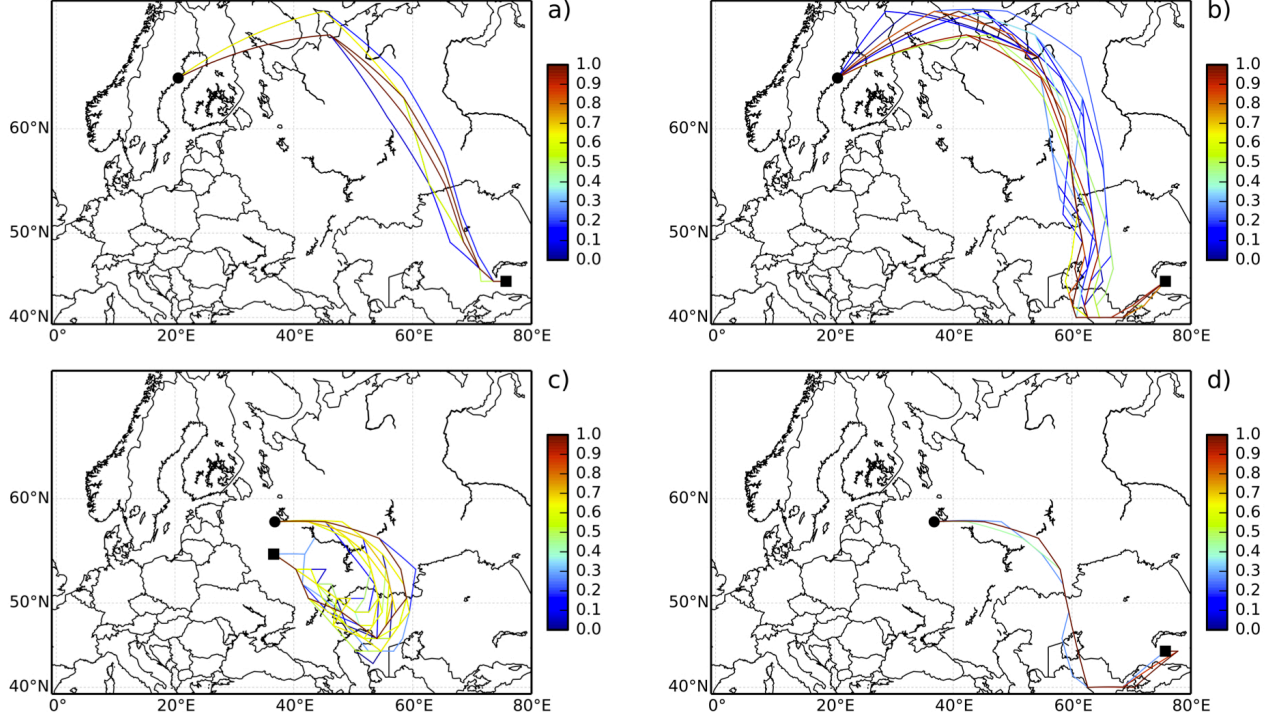


FIG. 7. All paths in  $\mathcal{K}_{IJ}^M(r=1, \epsilon=0.1)$  for different  $I, J$ , initial point  $I$  marked by a circle and final point  $J$  marked by a square. Panel a):  $M=8$  steps, with starting date July 25th 2011. Panel b):  $M=12$  steps, with starting date July 25th 2011. Panel c):  $M=11$  steps, with starting date July 20th 2011. Panel d):  $M=11$  steps, with starting date July 20th 2011. Same coloring scheme as in Figs. 3 and 4. For panels a) and b) probabilities ranging from  $10^{-5}$  to  $10^{-6}$  while for panels c) and d) from  $10^{-7}$  to  $10^{-8}$ . The maximum probability in each panel (dark red) corresponds to the MPP.

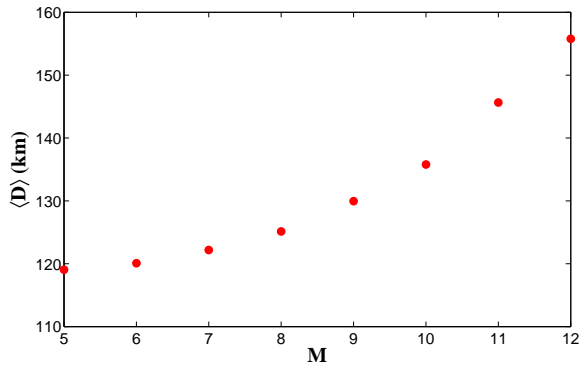


FIG. 8. Plot of the mean distance  $\mathcal{D}_{IJ}^M$  (Eq. (8)) as a function of  $M$  for  $r=1$  and  $\epsilon=0.1$ . The quantity is further averaged over all the HPPs starting on July 25th. Units are kilometers.

- <sup>19</sup>B. Trunday, L. Perthuis, S. Strebelle, J. D. Farrara, and C. R. Mechoso, “Dispersion properties of the flow in the southern stratosphere during winter and spring,” *Journal of Geophysical Research: Atmospheres* **100**, 13901–13917 (1995).
- <sup>20</sup>J. Lacasce, “Statistics from Lagrangian observations,” *Progress in Oceanography* **77**, 1–29 (2008).
- <sup>21</sup>R. Lumpkin and S. Elipot, “Surface drifter pair spreading in the North Atlantic,” *Journal of Geophysical Research: Oceans* **115**, C12017 (2010).
- <sup>22</sup>E. Ser-Giacomi, R. Vasile, E. Hernández-García, and C. López, “Most probable paths in temporal weighted networks: An application to ocean transport,” preprint arXiv 1411.6902 (2014).
- <sup>23</sup>M. Dellnitz, M. Hessel-von Molo, P. Metzner, R. Preis, and C. Schütte, “Graph algorithms for dynamical systems,” in *Analysis, Modeling and Simulation of Multiscale Problems*, edited by A. Mielke (Springer Verlag, Heidelberg, 2006) pp. 619–645.
- <sup>24</sup>N. Santitissadeekorn and E. Boltt, “Identifying stochastic basin hopping by partitioning with graph modularity,” *Physica D: Non-linear Phenomena* **231**, 95 – 107 (2007).
- <sup>25</sup>V. Rossi, E. Ser-Giacomi, C. López, and E. Hernández-García, “Hydrodynamic provinces and oceanic connectivity from a trans-

- port network help designing marine reserves,” *Geophysical Research Letters* **41**, 2883–2891 (2014).
- <sup>26</sup>E. Ser-Giacomi, V. Rossi, C. López, and E. Hernández-García, “Flow networks: A characterization of geophysical fluid transport,” preprint arXiv 1409.4171 (2014).
- <sup>27</sup>H. Kim and R. Anderson, “Temporal node centrality in complex networks,” *Physical Review E* **85**, 026107 (2012).
- <sup>28</sup>E. W. Dijkstra, “A note on two problems in connexion with graphs,” *Numerische Mathematik* **1**, 269–271 (1959).
- <sup>29</sup>H. H. Lentz, T. Selhorst, and I. M. Sokolov, “Unfolding accessibility provides a macroscopic approach to temporal networks,” *Physical Review Letters* **110**, 118701 (2013).
- <sup>30</sup>M. Matsueda, “Predictability of Euro-Russian blocking in summer 2010,” *Geophys. Res. Lett.* **38**, L06801 (2011).
- <sup>31</sup>E. Black, M. Blackburn, G. Harrison, B. Hoskins, and J. Methven, “Factors contributing to the summer 2003 European heatwave,” *Weather* **59**, 217–223 (2004).
- <sup>32</sup>S. Saha and coauthors, “The NCEP Climate Forecast System Reanalysis,” *Bull. Amer. Meteor. Soc.* **91**(8), 1015–1057 (2010).
- <sup>33</sup>A. Stohl, C. Forster, A. Frank, P. Seibert, and G. Wotawa, “Technical note: The Lagrangian particle dispersion model FLEXPART version 6.2,” *Atmos. Chem. Phys.* **5**, 2461–2474 (2005).
- <sup>34</sup>A. Stohl, H. Sodemann, S. Eckhardt, A. Frank, P. Seibert, and G. Wotawa, “The Lagrangian particle dispersion model FLEXPART version 8.2,” *FLEXPART user guide* (2011).